Solar Spectrum Photocatalytic Conversion of CO2 and Water Vapor Into Hydrocarbons Using TiO2 Nanoparticle Membranes

ARTICLE *in* APPLIED SURFACE SCIENCE · JANUARY 2014

Impact Factor: 2.71 · DOI: 10.1016/j.apsusc.2013.10.135

3 AUTHORS, INCLUDING:

Sanju Rani
International Advanced Research Centre fo…
11 PUBLICATIONS **399** CITATIONS

SEE PROFILE

Applied Surface Science 289 (2014) 203–208

Contents lists available at ScienceDirect

Applied Surface Science

journal homepage: www.elsevier.com/locate/apsusc

Solar Spectrum Photocatalytic Conversion of CO_2 and Water Vapor Into Hydrocarbons Using TiO_2 Nanoparticle Membranes

Sanju Rani[a,1], Ningzhong Bao[b], Somnath C. Roy[a,*,2]

[a] Materials Research Institute, The Pennsylvania State University, University Park, PA 16802, USA
[b] State Key of Laboratory of Materials-Oriented Chemical Engineering, Nanjing University of Technology, Nanjing 210009, P.R. China

ARTICLE INFO

Article history:
Received 11 June 2013
Received in revised form 13 October 2013
Accepted 21 October 2013
Available online 30 October 2013

Keywords:
TiO_2
Nano-particle membrane
CO_2 reduction
Photocatalysis
Hydrocarbon.

ABSTRACT

A viable option for recycling carbon dioxide is through the sunlight-powered photocatalytic conversion of CO_2 and water vapor into hydrocarbon fuels over highly active nanocatalysts. With photocatalytic CO_2 reduction sunlight, a renewable energy source as durable as the sun, is used to drive the catalytic reaction with the resultant fuel products compatible with the current hydrocarbon-based energy infrastructure. The use of co-catalyst (Cu, Pt)-sensitized TiO_2 nanoparticle wafers in the photocatalytic conversion of CO_2 and water vapor to hydrocarbon fuels, with optimal humidity levels and exposure times established. We also attempted to increase product formation by sputtering both co-catalysts on the nanoparticle wafer's surface, with the resulting product rates significantly higher than that of either the Cu or Pt coated samples. When the TiO_2 nanoparticle wafers are used in a flow-through membrane implementation we find a significant increase in product rates of formation, including methane, hydrogen, and carbon monoxide. We believe that nanocatalyst-based flow-through membranes are a viable route for achieving large-scale and low cost photocatalytic solar fuel production.

1. Introduction

The rise in atmospheric carbon dioxide levels resulting from the combustion of hydrocarbon fuels is of great concern due to its impact on global warming [1,2]. Consequently there is a broad effort across the globe to find alternative, renewable sources of energy. Generation of electricity from sunlight through the use of photovoltaic solar cells is well known [3,4], although more efficient devices at lower cost remain a continued objective. Solar fuels, that can be stored or transported as needed, represent a more challenging prospect for the renewable energy community. Hydrogen generation by water photoelectrolysis[5,6] offers intriguing prospects for a renewable fuel the combustion product of which is water, however hydrogen poses considerable challenges with respect to its storage, transportation, and use; to date large scale implementation of a hydrogen economy remains economically unfeasible.

Over the past several years we have explored the photocatalytic conversion of CO_2 and water vapor into hydrocarbon fuels, primarily methane- an ingredient that constitutes over 95% of natural gas, that are compatible with the current energy infrastructure. The solar driven photocatalytic conversion of CO_2 and water vapor into hydrocarbon fuels is a viable option for CO_2 recycling with minimal burden to the existing energy infrastructure. Since the 1979 report by Honda and coworkers[7] on the photocatalytic reduction of CO_2 in an aqueous solution, many research groups have investigated the mechanism and efficiencies of CO_2 reduction with a variety of semiconductors in either liquid[8–11] or gas phase[12–25]. Roy *et al.* [26] presents a recent review on the topic.

Photocatalysis requires a photo-active semiconductor in which a large number of electron-hole pairs are efficiently generated with the illumination of photons of appropriate energy[5]. Easily synthesized oxide-based photocatalysts such as TiO_2 have the advantage of being chemically and thermally stable[6]. Further, metal nanoparticles are needed to serve as electron sinks and/or active sites for CO_2 adsorption and reduction. In the recent work on gas phase CO_2 reduction by Varghese and co-workers[17] TiO_2 nanotube array samples, sensitized with Pt and Cu nanoparticles on the top surface, kept in specially designed photocatalytic reaction chambers filled with CO_2 and water vapor were exposed to outdoor sunlight to obtain, as main products, methane as well as syngas precursors hydrogen and CO.

In addition to the form and phase of the TiO_2 semiconductor 'backbone' and co-catalyst nanoparticles, other factors such as relative humidity and solar exposure duration play key roles in the gas phase reduction of CO_2. For example metallic nanoparticles, used

* Corresponding author.
E-mail address: somnath@iitm.ac.in (S.C. Roy).
[1] Present Address: Centre for Fuel Cell Technology, ARC International, IIT Madras Research Park, Phase 1, 2nd Floor, 6 Kanagam Road, Taramani, Chennai 600113, India
[2] Present Address: Environmental Nanotechnology Laboratory, Dept. of Physics, Indian Institute of Technology (IIT) Madras, Chennai 600036, India.,

0169-4332/$ – see front matter © 2013 Elsevier B.V. All rights reserved.
http://dx.doi.org/10.1016/j.apsusc.2013.10.135

to functionalize the TiO_2, tend to degrade faster when exposed to a high humidity environment leading to a reduction in the photoconversion efficiency. Similarly, samples exposed to solar radiation beyond an optimum duration encounter higher rates of back reactions with a corresponding decrease in product formation. In this work we examine the effects of relative humidity and solar exposure duration on the gas phase photocatalytic conversion of CO_2 using TiO_2 nanoparticle wafers functionalized with Cu and/or Pt nanoparticles.

2. Experimental

Nanoparticle wafers were fabricated using TiO_2 powder (Degussa-P25, 80% anatase- 20% rutile) having an average particle size of 25 nm. Polyethylene glycol (Fluka, PEG-2000), 5 wt. % of TiO_2, was used as a binder to make wafers mechanically robust. TiO_2 nanopowder and PEG were mixed in ethanol and grinded for 2 hours to ensure proper mixing. The resultant slurry was left for 10-12 h under a table lamp for drying at approximately 28 °C. A 25.4 mm diameter die and hydraulic press were used for pressing the dried powder into wafers by applying a pressure of 500 kg/cm^2. The pressed wafers, 300 μm to 500 μm thick, were annealed at 400 °C in air for 4 h to remove organics and volatile compounds.

The crystallinity and phase composition of the pressed wafers were determined using a Rigaku X-ray diffractometer. To confirm removal of volatile and organic compounds from the pressed wafers Fourier Transform Infra-Red spectroscopy was performed using a Brucker model IF66/S spectrometer in diffuse reflectance optics. The pore size of the TiO_2 wafers was estimated by gas adsorption/desorption kinetics using a Micromeritics Instruments surface area measurement system. Cu and/or Pt particles were deposited on the wafer surface using a Baltec DC sputtering system. The relative composition of Pt and Cu nanoparticles on the wafer surface with respect to TiO_2 was determined using a Perkin-Elmer XPS system.

Photocatalytic CO_2 reduction was performed in an indigenously designed 7.5 cm^3 stainless steel reaction chamber equipped with valves for filling and sealing of the chamber, a septum for gas sampling, and quartz window through which the sample was illuminated[17]. The relative humidity, RH, of the reaction chamber was controlled by mixing dry CO_2 and moist CO_2 (dry gas bubbled through de-ionized water) while keeping the total amount of CO_2 inside the reaction chamber constant. The relative humidity of the gas mixture was measured using an RH probe attached to a Keithley 6517 Electrometer. After placing the wafer inside the reaction chamber it was evacuated to a pressure of 10 mTorr and then flushed with CO_2 of desired RH for several minutes before the valves were closed (first the exit valve, then 10 s later the entrance valve). The total pressure of moisture contained CO_2 was kept close to that of atmospheric pressure in order to perform the photocatalytic reaction in ambient conditions. For testing the chamber was illuminated under AM 1.5G using a Class A solar simulator (Newport corporation), 100 mW/cm^2. Gas samples were analyzed using a Shimadzu GC 2014 gas chromatograph equipped with FID and TCD detectors. The possibility of sample contamination was investigated by performing photocatalytic CO_2 reduction experiments replacing water vapor with high purity helium; in all such cases only ≈ 1-2 ppm hydrocarbon levels were detected.

3. Results and Discussion

A flow-through configuration (Figure 1**a**) was implemented by raising the wafer off the bottom of the reaction chamber using a perforated Teflon spacer that allowed, but did not force, gas circulation through the wafer. To maximize the product output, the top surface of the wafer was sensitized with both Cu and Pt

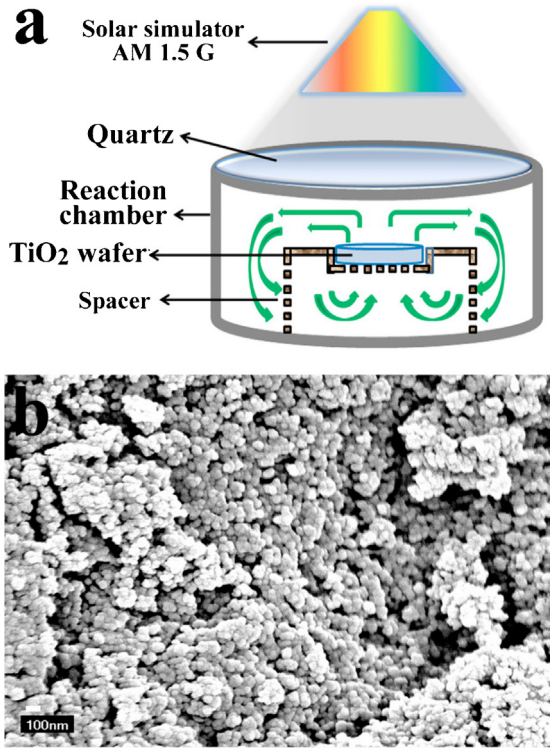

Figure 1. (a) Schematic diagram of photocatalytic flow-through membrane experiment. The cruved arrows denote circulation of the gases within the reaction chamber. (b) FESEM image of the nanoparticle wafer surface.

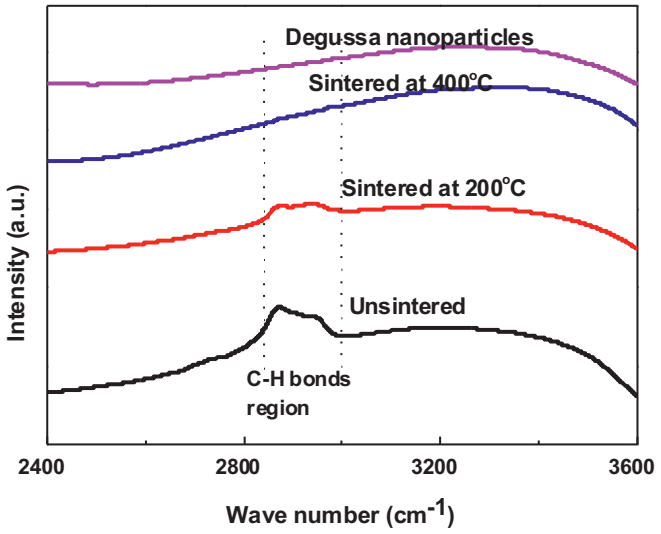

Figure 2. FTIR spectrum of Degussa nanoparticles, nanoparticle wafer before sintering and after sintering at 200 °C and 400 °C.

nanoparticles, each covering half of the surface area. The photocatalytic product formation rates from such a flow-through configuration has been presented later.

Figure 1**b** is a field emission scanning electron microscope (FESEM) image of the nanoparticle wafer surface. The TiO_2 nanoparticles are uniformly dispersed, forming a nanoporous structured film. FTIR spectra of the wafers under different sintering conditions are shown in Figure 2, with that for P-25 powder shown for comparison. The FTIR spectrum of the un-sintered wafer shows absorption in the 2800-3000 cm^{-1} range indicating trace organics. These absorption bands gradually disappear with sintering

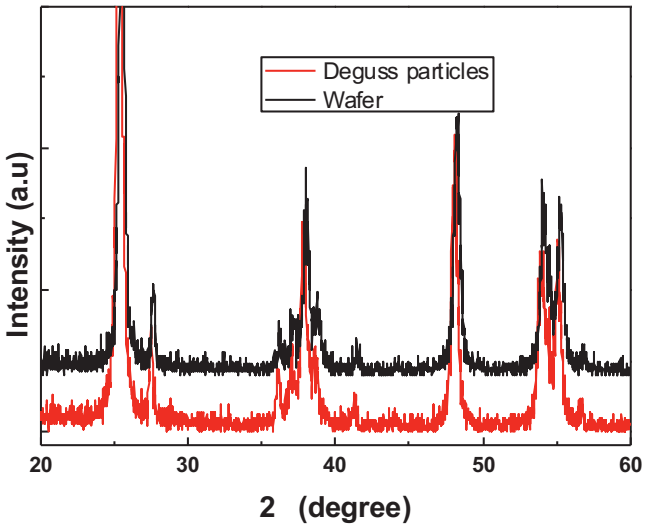

Figure 3. X-ray diffraction patterns of wafer sintered at 400 °C.

temperature; the spectrum of the wafer sintered at 400 °C for 4 h matches with that of the P-25 Degussa powder, indicating complete removal of the binder. Further increases in the sintering temperature were not attempted to avoid unintentional phase variation compared with the P-25 powder. Figure 3 shows the XRD patterns of Degussa P-25 TiO_2 powder and the TiO_2 wafer sintered at 400 °C for 4 h. As seen in the XRD patterns, wafer sintering did not induce an additional phase change, with all observed peaks similar to that of the P-25 powder. The pore size distribution of the wafers was measured using the BJH technique; the gas adsorption-desorption curves are shown in Figure 4**a**. A remarkable adsorption at high relative pressures suggests the presence of a high surface area nanoporous structure caused by the packed nanoparticles as indicated by the FESEM image (Figure 1**b**). The average pore size estimated from the adsorption-desorption curves was about 30 nm as seen in Figure 4**b**.

As mentioned by Varghese et al., [17] photo-generated holes help to ionize water and the electrons reduce CO_2. The photocatalytic reaction processes are chemically represented as:

$$TiO_2 + Solar\ Radiation = TiO_2^* + e^- + h^+$$

$$H_2O + h^+(Photo - generated\ holes\ from\ TiO_2) = OH^*(Radical) + H^+$$

$$2H^+ + 2e^-(Photo - generated\ electrons\ from\ TiO_2) = H_2$$

$$2CO_2 + 4e^- = 2CO + O_2$$

$$CO + 6e^- + 6h^+ = CH_4 + H_2O$$

The nanoparticles of metals (Pt/Cu), which act as co-catalysts, do not directly take part in these reactions; however they help towards the adsorption of gaseous species and the separation of the photo-generated electron-hole pairs. Hence, as a first experiment, TiO_2 wafers sensitized by either Pt or Cu co-catalyst nanoparticles were placed on the bottom of the photocatalytic reaction chambers in a 55% relative humidity CO_2 atmosphere and exposed to 1 h of AM 1.5G illumination. Figure 5a and Figure 5b show the gaseous reaction products as a function of sputter deposition times for, respectively, Cu and Pt deposition. Methane is found to be the major hydrocarbon product, while hydrogen and carbon monoxide are also observed. For Cu coated samples, Figure 5a, a sputtering time of 100 s (200 W power, 63 mA plasma current, 2 in diameter target) yielded a maximum methane production rate of 35 ppm/(cm^2·h),

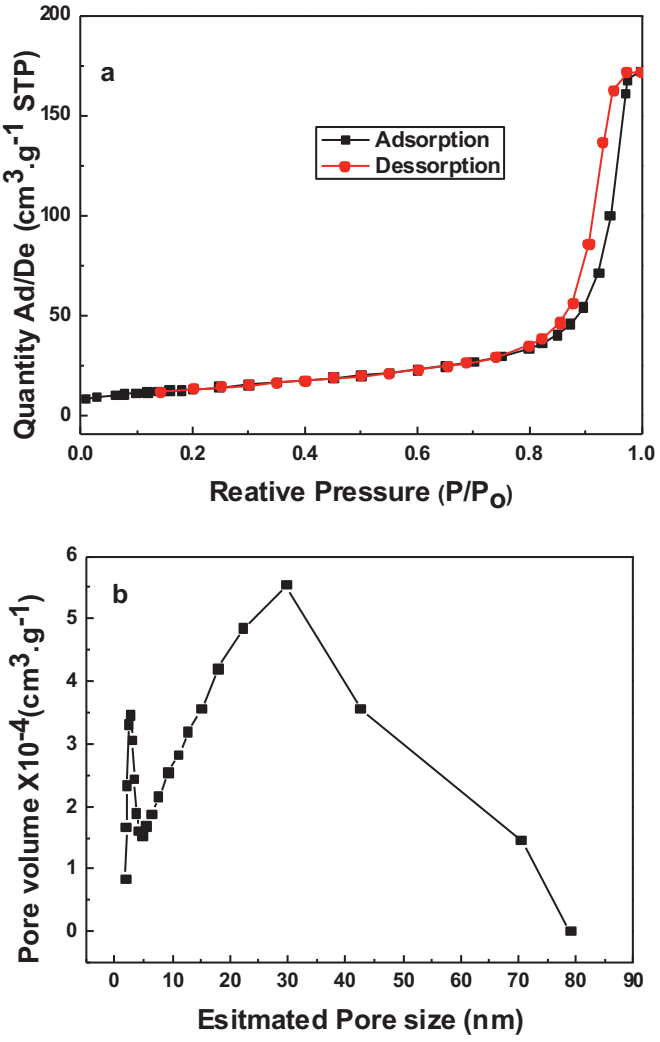

Figure 4. (a) Adsorption/Desorption (Ad/De) *vs.* relative pressure for pore size measurement. (b) Variation of pore volume with estimated pore size obtained from the absorption/desorption plot.

a value that decreased with further increases in sputtering time. The CO formation rate was found to increase with Cu sputtering time, a behavior attributed to enhanced CO_2 adsorption on the Cu sites and subsequent reduction to CO by electron transfer from the metal. However with increasing Cu coverage, depositions beyond 100 s, both light absorption and exposure of water vapor to the TiO_2 surface are reduced, which in turn reduces the possibility of H^+ ion formation through oxidation by the photo-generated holes. Hence in spite of the enhanced CO_2 reduction to CO, further Cu deposition and the corresponding reduced availability of H^+ ions decreases the rate of methane production. The amount of Cu relative to TiO_2 on the wafer surface after 100 s of sputtering, estimated by XPS with a sampling depth of approximately 8 nm, was determined to be 9.6%. Since a sputtering time of 100 s yielded a maximum methane formation rate for all further experiments utilizing Cu sensitization Cu was sputtered for 100 s.

The effect of Pt sputtering time (200 W, 63 mA, 2 in diameter target) on the product formation rates shows, Figure 5**b**, that a sputtering time of 8 s yields a maximum amount of methane and hydrogen. Therefore, for all further experiments involving Pt coated wafers, a sputtering time of 8 s was chosen. XPS analysis, ≈ 8 nm sampling depth, of wafers coated with Pt sputtered for 8 s showed that the amount of Pt relative to TiO_2 on the wafer surface was 8.7%.

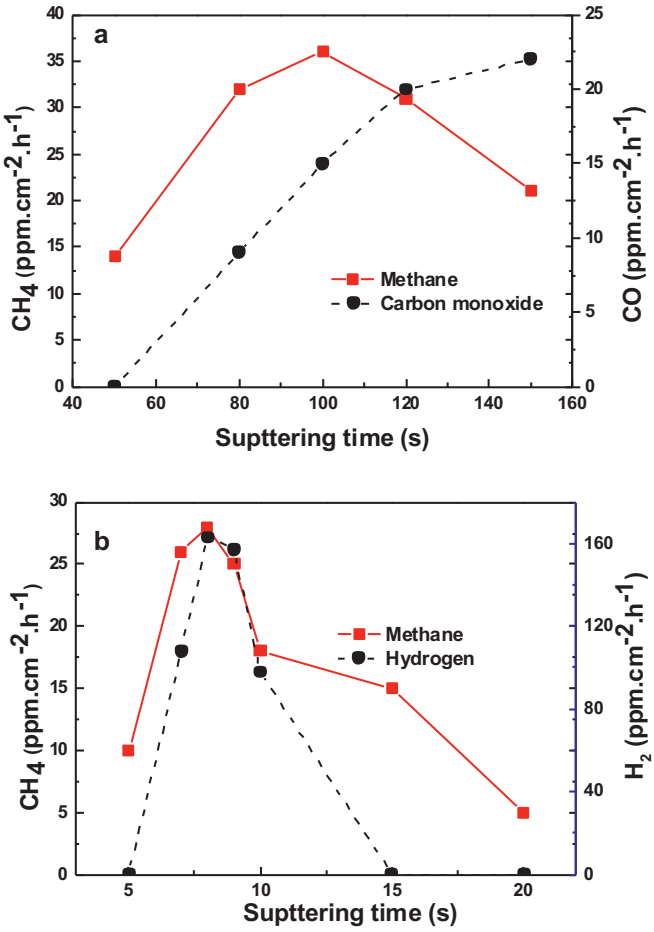

Figure 5. (a) Methane and carbon monoxide output with Cu- sputtered wafers. (b) Methane and hydrogen output with Pt- sputtered wafers.

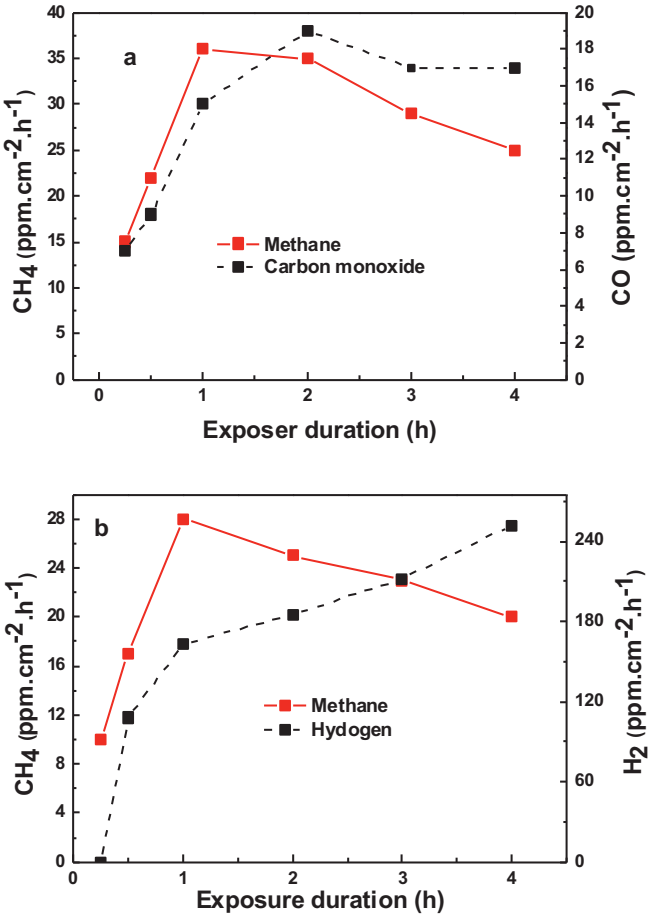

Figure 6. (a) Methane and carbon monoxide output as a function of illumination duration using Cu-sputtered wafers. (b) Methane and hydrogen output as a function of illumination duration using Pt-sputtered wafers.

To evaluate the reaction performance with time, wafers coated with Cu and Pt were illuminated for different durations, 0.25 h to 4 h. Figure 6**a** and Figure 6**b** show, respectively, time normalized product formation per unit area (ppm/(cm^2·h)) of Cu and Pt coated wafers. In both cases the methane yield reaches a maximum for 1 h exposure, beyond which it reduces with increasing exposure time. For the Cu coated sample the CO yield reaches a maximum value with 2 h exposure, and then reduces slightly with increasing exposure time. For the Pt coated samples the hydrogen yield increases with time reaching 250 ppm/(cm^2·h) with a 4 h exposure. Pt is a noble metal and its Fermi level is lower than that of the TiO_2. Hence the photo-excited electrons are easily separated from the corresonding holes in the photo-catalyst (TiO_2) and enter Pt, which act as an electron sink. This lowers the chances of electron-hole recombination. In a Pt-TiO_2 system under illumination, therefore, the holes can react with water to produce hydrogen ions, which, in turn, react with electrons to yield hydrogen molecule. As mentioned in the report by Kitano *et al.* (*Appl. Catal. A, 325, 2007, 1*), a Pt-TiO_2 system can work as a short-circuited electrochemical cell that promotes hydrogen evolution from water under the light irradiation. For the present experimental conditions the time dependence of the hydrocarbon product yield indicates that both Cu and Pt co-catalysts show maximum activity in the first hour of exposure followed by degradation thereafter.

CO_2 gas with moisture content ranging from 0% to 100% was tested in the reaction chamber. Figure 7**a** and Figure 7**b** show, respectively, the effect of relative humidity on product formation for wafers coated with Cu and Pt nanoparticles. Experiments with dry CO_2 on both Cu coated and Pt coated wafers yield less than 10 ppm/(cm^2·h) of methane and similar amounts of CO and hydrogen. For Cu coated samples, rates of both methane and CO reach a maximum at about 55% RH and decreases with higher RH values; yields at 100% RH are about 20 ppm/cm^2•h for methane and 9 ppm/(cm^2·h) for CO. A similar trend is observed for the methane yield in Pt coated samples, which begins with 5 ppm/cm^2•h at 0% RH, with a maximum yield of 32 ppm/(cm^2·h) at 55% RH and decreases to 15 ppm/(cm^2·h) at 100% RH. However, hydrogen production increases monotonically and reaches its maximum value of 200 ppm/(cm^2·h) at 100% RH. The optimum moisture content for maximum methane formation is about 55% RH and further increasing the water vapor content inside the reaction chamber leads to degradation of catalysts. With use of the samples in the CO_2 reduction chamber, visual inspection of the Cu sensitized wafers showed the Cu nanoparticles turned from metallic in appearance to dark colored as associated with copper oxide.

It has been shown that for gas phase photocatalytic conversion of CO_2 that product yields can be maximized by having both Cu and Pt nanoparticles deposited on the surface of the semiconductor photocatalyst [17]. Hence we attempted to increase product formation by sputtering Cu (100 s) on half of the wafer's surface and Pt (8 s) on the other half. The coatings of Pt and Cu were not overlapped in order to avoid the covering of one metal with the other. Figure 8 shows the product formation rates from a Cu-Pt sensitized wafer kept in a 55% RH CO_2 ambient and illuminated for 1 h; the methane yield reaches 49 ppm/(cm^2·h), significantly higher than that of either Cu or Pt coated samples.

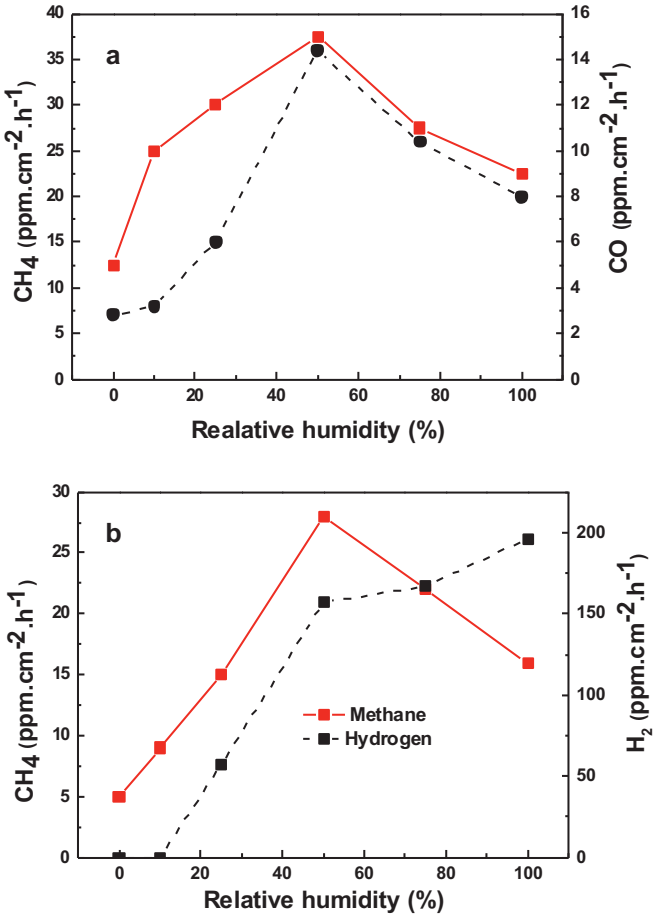

Figure 7. (a) Methane and carbon monoxide output for Cu sputtered samples as a function of relative humidity. (b) Methane and hydrogen output for Pt sputtered samples as a function of relative humidity.

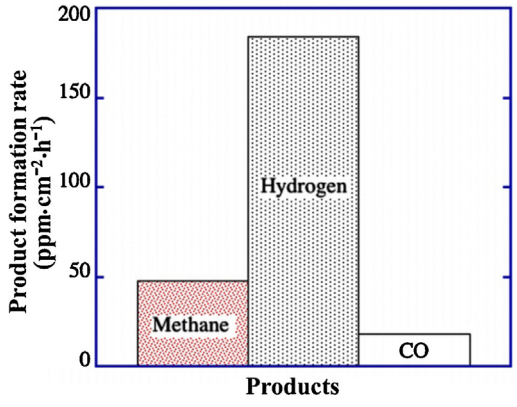

Figure 8. Product formation with wafer sensitization by both Pt and Cu nanoparticles.

In order to have a practical and efficient CO_2 conversion process, a dynamic system involving a flow-through configuration is essential, wherein CO_2 and water vapor can be passed through one end of a photocatalytic membrane exposed to solar radiation and hydrocarbon products are collected from the other end. Grimes and coworkers [17,27] conceived the idea of such a photocatalytic flow-through membrane using TiO_2 nanotube arrays. As shown the Fig. 1(a), we attempted to evaluate the effectiveness of nanoporous TiO_2 pellet as a flow-through membrane. Since the pellet was not transparent, light did not reach the other side (of the surface). Therefore, there was no "photo-catalytic" reaction expected on that side (bottom part) of the pellet. Referring to Fig. 1a, light from the solar simulator was incident on the top surface of the pellet (coated with Pt and Cu) and caused photo-catalytic reactions to take place; however, because of the lifted geometry and availability of micro-channels (randomly connected pores) in the pellet, the products could permeate through the pellet to the other side, reducing the chances of back-reactions. When the pellet was placed on the bottom of the reaction chamber, the reactants and products are always in close proximity to each other near the top surface and that was expected to enhance the back reaction rate. Furthermore, the other side of the disk was neither exposed to light nor coated with co-catalysts (Cu/Pt) and hence, this side did not take part in the photo-catalytic reactions. In this experiment, keeping the pellet in a CO_2 atmosphere with 55% RH and illuminated for 1 hr., which resulted in a 25% increase in product formation. In the case of methane, 62 ppm/(cm^2·h) was achieved as compared to 49 ppm/(cm^2·h) for the 'static' configuration when was the wafer was simply placed on the floor of the reactor. When converted to volumetric quantity, taking into account the volume of the chamber and STP conditions, 62 ppm/(cm^2·h) of methane amounted to about 3 nMol/cm^2.h. If the other side of the pellet had been exposed to light and taken part in the photo-catalytic reactions; then the effective product formation per unit surface area would have been reduced because of the increase in the available surface for photo-catalytic reactions. Therefore, we believe that, the increase in product formation could be attributed to the lifted geometry, in which the pellet acted like a flow-through membrane, giving way to the reaction products to be moved away and hence reducing the chances of back-reactions. The use of such wafers configured as flow-through membranes is a viable route for achieving large-scale and low cost photocatalytic solar fuel production.

4. Conclusion

Thin wafers made from P-25 Degussa TiO_2 powder sensitized with Cu and/or Pt nanoparticle co-catalysts have been explored for gas-phase photocatalytic reduction of CO_2. Sputtered layers of Cu and Pt co-catalysts were deposited on the wafer surface to enhance reaction rates, which were effectively zero when the co-catalysts were not used. We found that optimum amounts of co-catalyst loading on the wafer surface were approximately 9.6 at. % of Cu and 8.7 at % Pt while the presence of both co-catalysts improved overall reaction rates. Experiments to study the effect of relative humidity (RH) on CO_2 reduction revealed that the reduction products reached a maximum with a RH of 55%. Photocatalytic reaction rates were studied as a function of illumination duration with maximum product formation observed for 1 hr exposure. Longer illumination durations led to visible degradation of the metal co-catalysts and hence a reduction in the product formation rates.

In a passive, flow-through membrane configuration an approximately 25% increase in product output was achieved in comparison to the static configuration. Optimal membrane thickness and membrane pore size has yet to be determined. Greater porosity will allow a greater number of inter-connecting channels for co-catalyst sensitization as well as gas transport, while thicker membranes allow for greater light absorption. Uniform sensitization of the co-catalyst upon the entire surface of the photocatalytic semiconductor, via techniques such as microwave solvothermal [25] or atomic layer deposition (ALD), [28] should further enhance the photocatalytic reaction rates.

Acknowledgements

The authors thank Prof. Craig A. Grimes for useful discussion.

References

[1] W.R. Turner, M. Oppenheimer, D.S. Wilco, Nature. 462 (2009) 78–279.
[2] R.A. Kerr, Science. 318 (2007) 1230–1231.
[3] S. Licht, Nature. 330 (1987) 148–151.
[4] K. Varghese, M. Paulose, C.A. Grimes, Nature Nanotechnology. 4 (2009) 592–597.
[5] A. Fujishima, K. Honda, Nature. 238 (1972) 38–39.
[6] C.A. Grimes, O.K. Varghese, S. Ranjan, Light, Water, Hydrogen The Solar Generation of Hydrogen by Water Photoelectrolysis, Springer, New York, 2007.
[7] T. Inoue, A. Fujishima, S. Konishi, K. Honda, Nature. 277 (1979) 637–638.
[8] M. Halmann, M. Ulman, B.A. Blajeni, Sol. Energy. 31 (1983) 429–431.
[9] R.L. Cook, R.C. Macduff, A.F. Sammells, J. Electrochem. Soc. 135 (1988) 3069–3070.
[10] K. Adachi, K. Ohta, T. Mijuma, Sol. Energy. 53 (1994) 187–190.
[11] M. Anpo, K. Chiba, J. Mol. Catal. 74 (1992) 207–212.
[12] K.R. Thampi, J. Kiwi, M. Graetzel, Nature. 327 (1987) 506–508.
[13] J. Melsheimer, W. Guo, D. Ziegler, M. Wesemann, R. Schlogl, Catal. Lett. 11 (1991) 157–168.
[14] J.C.S. Wu, T.-H. Wu, T. Chu, H. Huang, D. Tsai, Top. Catal. 47 (2008) 131–136.
[15] S.S. Tan, L. Zou, E. Hu, Sci. Technol. Adv. Mater. 9 (2007) 89–92.
[16] C.C. Lo, C.H. Hung, C.S. Yuan, J.F. Wu, Sol. Energy Mater. Sol. Cells. 91 (2007) 1765–1774.
[17] O.K. Varghese, M. Paulose, T.J. LaTempa, C.A. Grimes, Nano Lett. 9 (2009) 731–737.
[18] Q. Liu, Y. Zhou, J. Kou, X. Chen, Z. Tian, J. Gao, S. Yan, Z. Zou, J. Am. Chem. Soc. 132 (2010) 14385–14387.
[19] M.A. Asi, C. Hea, M. Su, D. Xia, L. Lin, H. Deng, Y. Xiong, R. Qiu, X.-Z. Li, Catal. Today. 175 (2011) 256–263.
[20] Y.T. Liang, B.K. Vijayan, K.A. Gray, M.C. Hersam, Nano Lett. 11 (2011) 2856–2860.
[21] H. Shi, T. Wang, J. Chen, C. Zhu, J. Ye, Z. Zou, Catal Lett. 141 (2011) 525–530.
[22] G. Xi, S. Ouyang, J. Ye, Chem. Eur. J 17 (2011) 9057–9061.
[23] T. Yui, A. Kan, C. Saitoh, K. Koike, T. Ibusuki, O. Ishitani, ACS Appl. Mater. Interfaces. 3 (2011) 2594–2600.
[24] Y. Zhou, Z. Tian, Z. Zhao, Q. Liu, J. Kou, X. Chen, J. Gao, S. Yan, Z. Zou, ACS Appl. Mater. Interfaces. 3 (2011) 3594–3601.
[25] X. Feng, J.D. Sloppy, T.J. LaTempa, M. Paulose, S. Komarneni, N. Bao, C.A. Grimes, J. Mater. Chem. 21 (2011) 13429–13433.
[26] S.C. Roy, O.K. Varghese, M. Paulose, C.A. Grimes, ACS Nano. 4 (2010) 1259–1278.
[27] K. Shankar, J.I. Basham, N.K. Allam, O.K. Varghese, G.K. Mor, X. Feng, M. Paulose, J.A. Seabold, K.S. Choi, C.A. Grimes, J. Phys. Chem. C 113 (2009) 6327–6359.
[28] A. Johansson, T. Torndahl, L.M. Ottosson, M. Boman, J.-O. Carlsson, Materials Science and Engineering C. 23 (2003) 823–826.